Supporting Information

Experimental Relaxivities

Supporting Table S1. Transverse Relaxivities in Plasma $(s^{-1}/(mmol(CR)/L(plasma)))^{+}$

	1.5 T				3.0 T			
	r_2		r_2^*		r_2		r_2^*	
gadobenate	6.1	(5.9,6.4)‡	7.5	(7.2,7.8)	6.2	(6.0,6.5)	8.7	(7.0,10.3)
gadoteridol	3.9	(3.8,4.0)	4.5	(4.3,4.8)	3.9	(3.8,4.0)	5.3	(3.7,7.0)
gadofosveset	11.2	(9.6,12.8)	15.6	(13.9,17.3)	10.6	(8.9,12.3)	17.0	(14.9,19.2)
gadobutrol	4.4	(4.3,4.6)	5.4	(4.7,6.0)	4.4	(4.3,4.6)	5.4	(5.2,5.6)

+Relaxivities determined by best fittings with the linear expression $R_2^{(*)} = r_2^{(*)}[CR_p] + 5\ s^{-1}$ over $[CR_e]$ range from 1.6 to 28 mM.
‡Confidence intervals from the linear fittings are listed in parentheses.

Supporting Table S1. Water proton transverse relaxivities (r_2 and r_2*) in plasma ($s^{-1}/(mmol(CR)/L(plasma))$) at 1.5 and 3.0 T. Relaxivities were determined by best fittings with the linear expression $R_2^{(*)} = r_2^{(*)}[CR_e] + 5\ s^{-1}$. Data were fit over the concentration $[CR_e]$ range from 1.6 to 28 mmol(CR)/L(plasma). Confidence intervals from the linear fittings are listed in parentheses.

Supporting Table S2. Transverse Relaxivities in Blood $(s^{-1}/(mmol(CR)/L(blood)))^{+}$

	1.5 T				3.0 T			
	r_2		r_2^*		r_2		r_2^*	
gadobenate	6.8	(6.5,7.2) ‡	22.5	(21.8,23.3)	10.6	(9.8,11.5)	44.9	(41.9,47.9)
gadoteridol	5.9	(5.7,6.1)	23.6	(21.8,25.5)	10.5	(10.0,10.9)	50.3	(44.8,55.7)
gadofosveset	9.4	(8.1,10.7)	27.5	(26.5,28.5)	12.0	(10.0,14.0)	47.2	(46.3,48.2)
gadobutrol	6.7	(6.5,7.0)	22.1	(20.4,23.8)	10.9	(10.0,11.7)	50.9	(46.4,55.4)

+Relaxivities determined by best fittings with the linear expression $R_2^{(*)} = r_2^{(*)}[CR_b] + 5\ s^{-1}$ over $[CR_b]$ range from 1 to 18 mM.
‡Confidence intervals from the linear fittings are listed in parentheses.

Supporting Table S2. Water proton transverse relaxivities (r_2 and r_2*) in blood ($s^{-1}/(mmol(CR)/L(blood))$) at 1.5 and 3.0 T. Relaxivities were determined by best fittings with the linear expression $R_2^{(*)} = r_2^{(*)}[CR_e] + 5\ s^{-1}$. Data were fit over the concentration $[CR_b]$ range from 1 to 18 mmol(CR)/L(blood). Confidence intervals from the linear fittings are listed in parentheses.

Additional Simulations

Additional simulations were run to explore the effects of: 1) potential cell alignment by the magnetic field ($\mathbf{B_0}$), and 2) the Lorentz cavity correction. The results are reported here. Comparison of these simulations with the experimental results makes it clear the cells were not substantially field-aligned during our acquisitions, and that the Lorentz cavity effect is manifest in experimental data.

Background: Simulations with randomly oriented cells

Our simulations assume the discoid RBCs were randomly oriented with respect to the $\mathbf{B_0}$ direction during our data acquisitions. However, when intra- and extracellular magnetic susceptibilities differ, $\mathbf{B_0}$ has the potential to orient non-spherical cells. The cellular angular distribution is important because it determines the intracellular resonance frequency distribution. Intra- and extracellular frequency distributions sensed during 6000 random walks through an ensemble of randomly oriented cells are shown in **Supporting Figure S1**. These spectra are similar to those predicted in Fig. 1. The powder pattern shape of the intracellular spectrum results from the random cellular orientation. As we will see below, the absolute and relative intra- and extracellular resonance frequencies are governed by Lorentz cavity effects. The extracellular spectrum is centered at $\chi_e/3$ ppm (Eq. [5]), which is -217 Hz for $[CR_b]$ = 8 mM and 3T. For illustration, the instantaneous resonance frequency time-course and the accumulated precessional phase for a single water proton spin during an example random walk through the ensemble are plotted in the left and right panels of **Supporting Figure S2**, respectively. This is for a FID; there are no SE phase reversals.

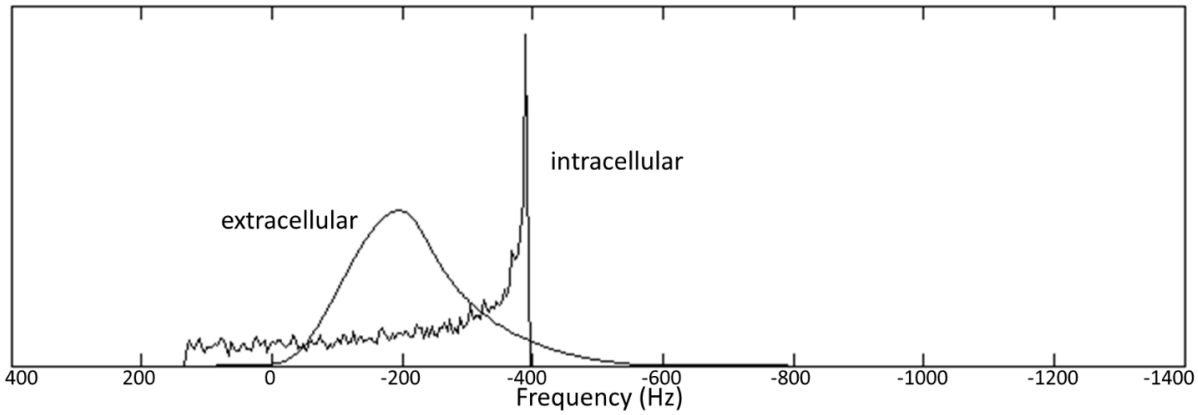

Supporting Figure S1. The distributions of resonance frequencies sensed during random walks through a cell ensemble. This spectrum is for randomly oriented erythrocytes, $[CR_b]$ = 8 mM and B_0 = 3T.

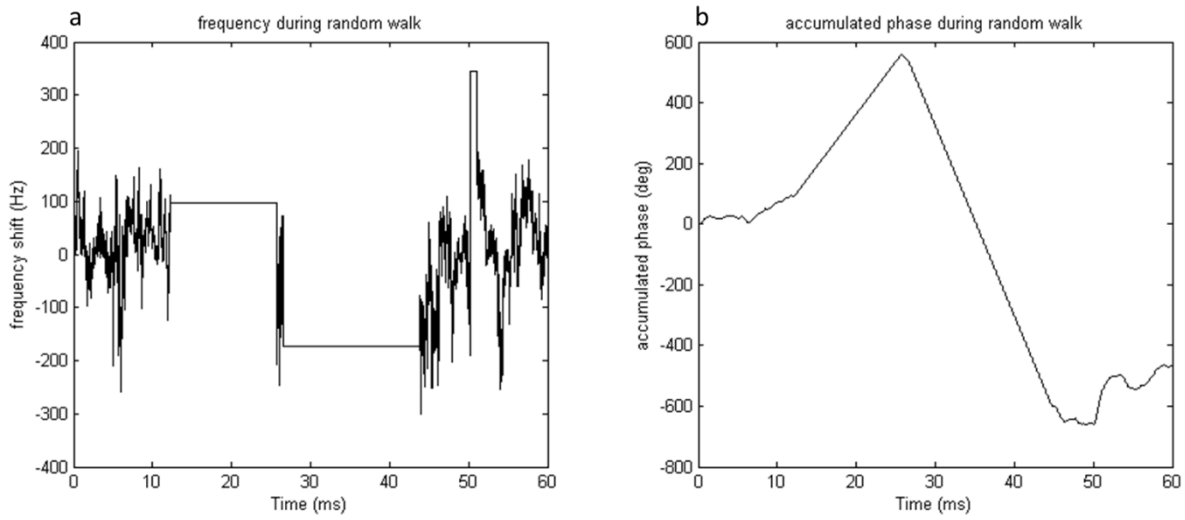

Supporting Figure S2. Example a) resonance frequency time-course and b) accumulated precessional phase trajectory of a single water proton during a random walk through an ensemble of randomly oriented erythrocytes; $[CR_b]$ = 8 mM and B_0 = 3T. This water molecule started in extracellular space and entered, and exited, three erythrocytes (a, horizontal line segments) with different orientations. In the extracellular space, the water proton experiences rapid fluctuations centered about zero frequency shift (relative to $D_e = \chi_e/3$; -217 Hz in this case; Eq. [5]). Thus, while extracellular, it accumulated phase much more slowly than while it was intracellular.

Simulations with magnetic field-aligned cells

As noted in the text, the extent of red blood cell alignment by $\mathbf{B_0}$ at clinical magnetic field strengths has been controversial. Thus, we simulated the effect of the limiting case of complete cell alignment (*i.e.*, all cell normals perpendicular to the $\mathbf{B_0}$ direction) to compare with the experimental results. The intra- and extracellular resonance frequency distributions sensed are shown in **Supporting Figure S3**. In this case, all intracellular spins experience the identical resonance frequency, while the extracellular spin frequencies are unaffected. Completely sampled (continual) simulated signal intensity decays (with $k_{io} = 100\ s^{-1}$) are shown in **Supporting Figure S4**. It is clear the decay from the "aligned cell" simulation (light gray curve) does not match the experimental data (filled circles), whereas that from the randomly oriented cell ensemble (black curve) does. Thus, we conclude the cells were not substantially aligned by $\mathbf{B_0}$ during our experiments.

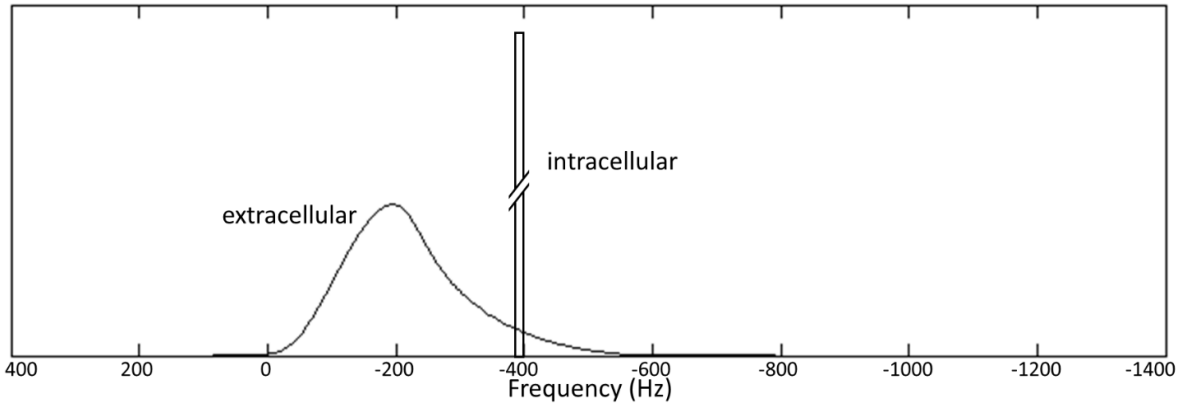

Supporting Figure S3. The distributions of resonance frequencies sensed during random walks through a cell ensemble. This intracellular spectrum is for erythrocytes with all ellipsoid normals perpendicular to the $\mathbf{B_0}$ direction, $[CR_b] = 8$ mM and $B_0 = 3$T. The intracellular resonance frequency is $\chi_i/3$ ppm ($\phi = 90^o$, Eq. [6]; -391 Hz, here) for all intracellular water protons.

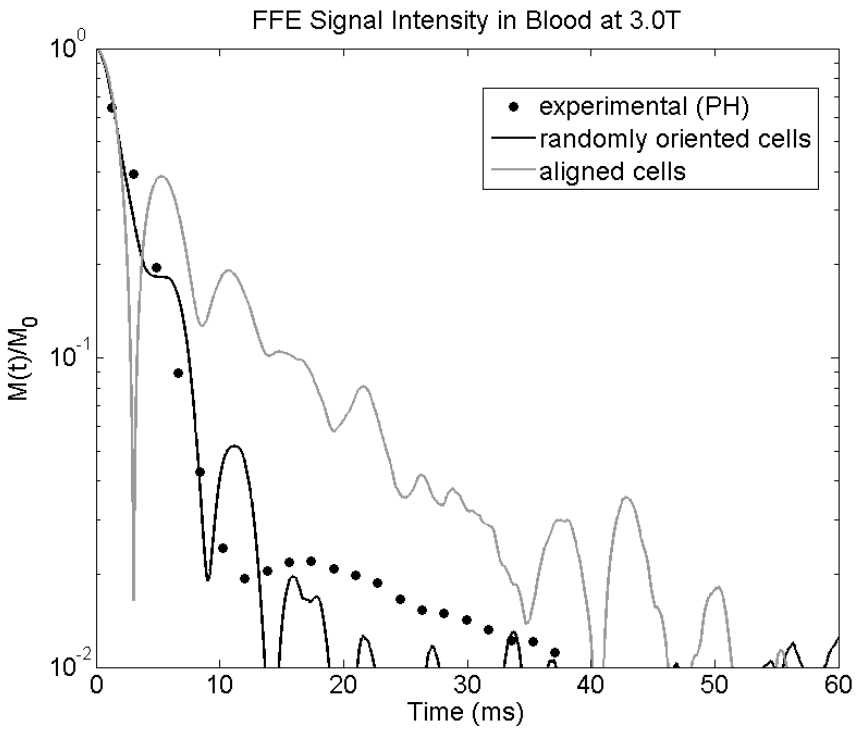

Supporting Figure S4. Semilogarithmic plots of completely sampled (continual) simulated signal intensity decays from samples with randomly oriented cells (dark curve) and completely aligned cells (light curve); $k_{io} = 100\ s^{-1}$, $[CR_b] = 8$ mM and $B_0 = 3$T. The aligned cell simulated FID (light curve) exhibits slower decay than the experimental data (filled circles), while the randomly oriented cell simulated FID matches them quite closely.

Simulations neglecting the Lorentz cavity

The Lorentz cavity is a construct to account for cancellation of local (on the molecular scale) magnetic dipole interactions with the resonant spin. Neglecting it shifts the intra- and extracellular resonance frequency positions from those in Fig. A1 by $2\chi_i/3$ and $2\chi_e/3$ ppm, respectively. This neglect has often been unintentional in published reports. Our simulations offer the rare opportunity to demonstrate the effect of neglecting the Lorentz cavity.

Example intra- and extracellular resonance frequency distributions when the Lorentz cavity is neglected are displayed in **Supporting Figure S5**. Both spectra are displaced to lower frequencies than is the case in Fig. A1, where all other factors are the same. However, the displacements are by different amounts; intracellular frequencies have a larger negative shift. This results in a broader resonance frequency span for water molecule spins in the erythrocyte ensemble. Completely sampled (continual) simulated and experimental signal intensity decays (with k_{io} = 100 s^{-1}) are shown in **Supporting Figure S6**. When the Lorentz cavity is neglected (light curve), the FID decreases much more rapidly than the experimental results, while the simulation that includes the cavity (black curve) agrees very well. Thus, we conclude the Lorentz cavity must be included to accurately reflect experimental measurements. The imaginary construct accounts for a very real effect.

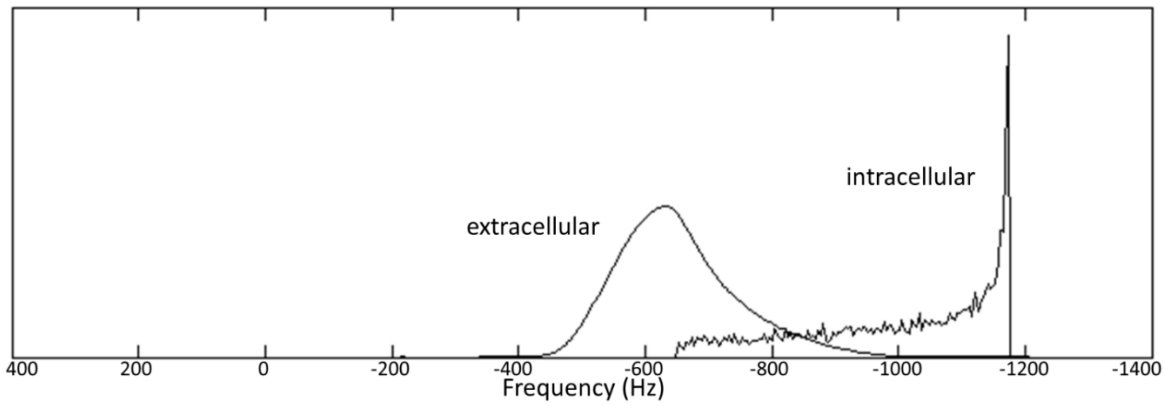

Supporting Figure S5. The distributions of resonance frequencies sensed during random walks through an ensemble of randomly oriented cells. This spectrum was obtained when the Lorentz cavity was neglected; for $[CR_b]$ = 8 mM and B_0 = 3T. Notice both intra- and extracellular distributions are shifted to lower frequency compared to the case including the Lorentz cavity (Fig. A1), but by different amounts. Thus, if the Lorentz cavity is neglected, water proton spins experience a broader range of frequencies.

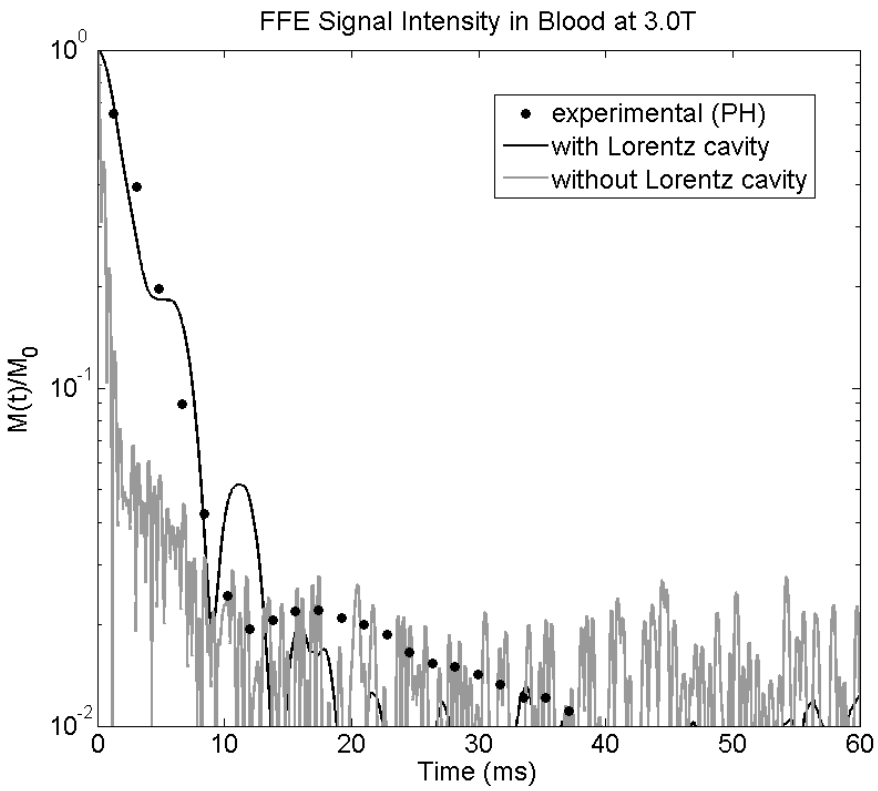

Supporting Figure S6. Semilogarithmic plots of completely sampled (continual) simulated signal intensity decays with (dark curve) and without (light curve) the Lorentz cavity correction; for k_{io} = 100 s^{-1}, [CR_b] = 8 mM and B_0 = 3T. The "no Lorentz cavity" simulated FID exhibits more rapid decay than the experimental data (filled circles) and very high frequency modulations. On the other hand, the signal decay including the Lorentz cavity correction matches the experimental data (filled circles) quite well.